Disturbances in bone largely predict aortic calcification in an alternative rat model developed to study both vascular and bone pathology in chronic kidney disease

Original Article

Disturbances in bone largely predict aortic calcification in an alternative rat model developed to study both vascular and bone pathology in chronic kidney disease†

Ellen Neven[1] PhD, Rida Bashir-Dar[1] MSc, Geert Dams[1], Geert J Behets[1] PhD, Anja Verhulst[1] PhD, Monique Elseviers[2] PhD, Patrick C D'Haese[1*] PhD.

[1]Laboratory of Pathophysiology, Department of Biomedical Sciences, University of Antwerp, Belgium

[2] Department of Nursing Sciences, Faculty of Medicine and Public Health, University of Antwerp, Antwerp, Belgium

* Corresponding author and offprint request:
Patrick C. D'Haese, PhD
Laboratory of Pathophysiology
University of Antwerp, Campus Drie Eiken
Universiteitsplein 1
B-2610 Wilrijk
Tel: +32-3 2652599, Fax: +32-3 2652592
patrick.dhaese@uantwerpen.be

Disclosure: The authors have nothing to disclose.

†This article has been accepted for publication and undergone full peer review but has not been through the copyediting, typesetting, pagination and proofreading process, which may lead to differences between this version and the Version of Record. Please cite this article as doi: [10.1002/jbmr.2585]

Initial Date Submitted April 27, 2015; Date Revision Submitted June 19, 2015; Date Final Disposition Set June 21, 2015

Journal of Bone and Mineral Research

DOI 10.1002/jbmr.2585

Abstract

As current rat models used to study chronic kidney disease (CKD)-related vascular calcification show consistent but excessive vascular calcification and chaotic, immeasurable bone mineralization due to excessive bone turnover, they are not suited to study the bone-vascular axis in one and the same animal. Since vascular calcification and bone mineralization are closely related to each other, an animal model in which both pathologies can be studied concomitantly is highly needed.

CKD-related vascular calcification in rats was induced by a 0.25% adenine/low vitamin K diet. To follow vascular calcification and bone pathology over time, rats were killed at week 4, 8, 10, 11 and 12. Both static and dynamic bone parameters were measured. Vascular calcification was quantified by histomorphometry and measurement of the arterial calcium content.

Stable, severe CKD was induced along with hyperphosphatemia, hypocalcemia as well as increased serum PTH and FGF23. Calcification in the aorta and peripheral arteries was present from week 8 of CKD onwards. Four and 8 weeks after CKD, static and dynamic bone parameters were measurable in all animals, thereby presenting typical features of hyperparathyroid bone disease. Multiple regression analysis showed that the eroded perimeter and mineral apposition rate in the bone were strong predictors for aortic calcification.

This rat model presents a stable CKD, moderate vascular calcification and quantifiable bone pathology after 8 weeks of CKD and is the first one that lends itself to study these main complications simultaneously in CKD in mechanistic and intervention studies.

Key words: chronic kidney disease – vascular calcification – bone disease – mineral abnormalities – rat model

Introduction

Vascular calcification and bone pathology are two complications of chronic kidney disease (CKD) with a major impact on mortality (1-3). As vascular calcification and bone disease are both hallmarks of CKD and related to each other (4;5), a new animal model in which both pathologies can be studied concomitantly is needed, particularly to study the effect of therapeutic compounds on the evolution of pathological arterial calcification as well as on (physiological) bone metabolism. Current strategies for treatment of vascular calcification in CKD mainly consist of controlling mineral disturbances such as hyperphosphatemia and secondary hyperparathyroidism. Despite the fact that these treatments have proven to reduce arterial calcification to some extent (3;6-8), research on alternative molecules that directly target the calcification process continues. Arterial calcification is induced by a host of promoters and a lack of inhibitors which makes it difficult to control the various provocative factors by current treatment strategies such as phosphate binding agents and calcimimetics. An innovative therapeutic approach implying the direct interference with the mineralization process in the vessel wall, independently of the causal factors involved, creates new opportunities. However, targeting the calcification process itself in the vessel wall entails the possible interference of the compound with bone mineralization. As such, for the therapeutic evaluation of compounds on CKD-related pathological vascular calcification, it is also a prerequisite to examine and exclude whether these agents negatively affect physiological bone mineralization.

To study CKD-related vascular calcification, the 0.75% adenine/low protein rat model is commonly used (9;10). However, as it shows consistent but excessive vascular calcification and chaotic and immeasurable bone mineralization due to the excessive bone turnover, it is less suited to study the bone-vascular axis in one and the same animal. Moreover, with the conventional model partial restoration of renal dysfunction after stop of adenine administration complicates evaluation of progression/reversal of established arterial calcification in intervention studies. On the other hand,

to study uremia-related bone disease, the well-established 5/6th nephrectomy model is usually applied, nevertheless, calcification in the arteries does not develop unless supra-physiological vitamin D concentrations are administered.

In view of this, the current study aims to optimize a modified rat model for CKD-related vascular calcification and bone pathology which would make it feasible to evaluate treatment strategies on both arterial calcification and CKD-related bone pathology simultaneously.

Methods

Study design

All experimental procedures were performed according to the National Institutes of Health Guide for the Care and Use of Laboratory Animals 85-23 (1996) and approved by the University of Antwerp Ethical Committee for Animal Experiments.

In the present study, 53 male Wistar rats of 8 weeks old were included (Iffa Credo, Brussels, Belgium). Animals were housed two per cage, exposed to a 12h light/dark cycle and had free access to food and water. An equilibration period of 4 weeks was provided to ensure a body weight of approximately 350 g at the start of the study. Subsequently, rats were maintained either on a control diet with low vitamin K (0.2 mg/kg VitK, 1% Ca, 1% P, 1 IU/g vitamin D and 6% protein) or an adenine diet with low vitamin K to induce CKD and vascular calcification (0.25% adenine, 0.2 mg/kg VitK, 1% Ca, 1% P, 1 IU/g vitamin D and 6% protein) (SSNIFF Spezialdiäten, Soest, Germany). To evaluate the onset and further progression of vascular calcification and bone disease over time, CKD rats on an adenine diet were killed at week 4 (n=8), 8 (n=8), 10 (n=10), 11 (n=10) and 12 (n=9). Animals with normal renal function fed a control diet were sacrificed at the end of the study, i.e. week 11 (n=8). Every two weeks, control rats and CKD rats were placed in metabolic cages to collect urine samples, followed by blood sampling via the tail vein. All animals received an intraperitoneal injection of 30 mg/kg tetracycline and demeclocycline at 7 and 3 days before sacrifice, respectively, to allow histomorphometric analysis of a series of dynamic bone parameters.

At sacrifice, rats were exsanguinated through the retro-orbital plexus after anesthesia with sodium pentobarbital (Nembutal, Ceva Santé Animale, France) 60 mg/kg via intraperitoneal injection.

Biochemical analyses

Serum creatinine was determined according to the Jaffé method. Total calcium in serum and urine was measured with flame atomic absorption spectrometry (Perkin-Elmer, Wellesley, MA, USA) after appropriate dilution in 0.1% $La(NO_3)_3$ to eliminate chemical interference. Serum and urinary phosphorus were measured using the Ecoline®S Phosphate kit (DiaSys, Germany). Serum iPTH (Immutopics, San Clemente, CA, USA) and FGF23 (Kainos Laboratories, Tokyo, Japan) levels were determined by use of an ELISA kit.

Evaluation of vascular calcification

After isolation of the thoracic aorta, the tissue was fixed in neutral buffered formalin for 90 minutes and cut into sections of 2-3 mm. These sections were embedded upright in a paraffin block and 4 µm sections were stained for calcification with Von Kossa's method and counterstained with haematoxylin and eosin. The % of calcified area was calculated using Axiovision image analysis software (Release 4.5,Carl Zeiss, Oberkochen, Germany) in which two color separation thresholds measure the total tissue area and the Von Kossa positive area. After summing both absolute areas, the % of calcified area was calculated as the ratio of the Von Kossa positive area versus the total tissue area.

The proximal part of the abdominal aorta and the left carotid and femoral artery were isolated and weighed on a precision balance. Subsequently, the samples were digested in 65% HNO_3 at 60°C overnight. The calcium content of the each artery was measured with flame atomic absorption spectrometry and expressed as mg calcium/g wet tissue.

Bone histomorphometry

The left tibia of each animal was isolated and cleared of surrounding tissue. After fixation in 70% ethanol overnight, the left tibia was further processed for bone histomophometric analysis: tibias were dehydrated and embedded in 100% methylmetacrylate (Merck, Hohenbrunn, Germany). Five µm thick sections were Goldner stained for visualization and measurement of total bone area, mineralized bone area, osteoid width and area, osteoblast perimeter, eroded perimeter and osteoclast perimeter which were quantified with Axiovision image analysis software (Release 4.5, Carl Zeiss, Oberkochen, Germany). Ten µm thick unstained sections of the tibia were used to measure distance between and length of double tetracycline and demeclocycline labels by fluorescence microscopy. Out of these primary data, additional histological bone parameters and dynamic bone parameters were calculated according to Parfitt et al (11).

mRNA expression analyses on aortic tissue

Total mRNA of the distal part of the abdominal aorta was extracted using the RNeasy Fibrous Tissue mini kit (Qiagen, Hilden, Germany) and reverse transcribed to cDNA by the High Capacity cDNA archive kit (Applied Biosystems, Foster City, CA, USA). Real time polymerase chain reaction (PCR) with an ABI Prism® 7000 Sequence Detection System (Applied Biosystems) based on Taqman fluorescence methodology was used for mRNA quantification. Taqman probe and primers were purchased as Taqman® gene expression assays-on-demand from Applied Biosystems for glyceraldehyde 3-phosphate dehydrogenase (GAPDH) (Rn99999916_s1), FGF23 (Rn00590709_m1), FGF18 (Rn00433286_m1), FGFR1 (Rn00577234_m1), FGFR3 (Rn00584799_m1), Klotho (Rn00580123_m1), prelamin A (Rn01750886_m1), FACE-1 (Rn01749372_m1), SOST (Rn00577971_m1). The expression of each tested gene was analyzed in triplicate for each sample and normalized to the expression of the house keeping gene GAPDH. Gene expression was calculated with the comparative CT method using aortas of control rats with normal renal function as calibrator samples.

Statistics

Results are expressed as mean ± standard deviation unless otherwise indicated. Non-parametric statistical analyses were performed with SPSS 20.0 software. Statistical differences between groups were investigated with Kruskall-Wallis test followed by Mann Whitney-U test. Comparison of time-points was performed with a Friedman related samples test, followed by a Wilcoxon signed ranks test. Bonferroni correction was applied when appropriate.

A Spearman's rho univariate correlation analysis was done between aortic calcium content and all biochemical and static and dynamic bone parameters measured. Based on significant univariate analysis correlations, multiple regression analysis on ranked data was performed to assess the relationship between aortic calcification and bone parameters. $P < 0.05$ was considered significant.

Results

Induction of chronic renal failure in rats by a continuous exposure to a low dietary adenine dose results in a low overall mortality of 7.5%; only 4 CKD rats died before the planned sacrifice. Two CKD rats died at week 8, one at week 10 and one rat died two days before sacrifice at week 12.

Renal impairment and mineral abnormalities

Serum and urinary parameters of renal function and mineral metabolism are presented in Table 1. Continuous administration of 0.25% dietary adenine led to significant doubling of serum creatinine concentrations after 2 weeks. Renal failure further progresses with maximal serum creatinine levels up to 5 mg/dl after 6 weeks of renal impairment. Stabilization of this parameter for renal function was seen afterwards, indicating the manifestation of severe, but stable chronic renal failure. In line with these results, after 6 weeks of CKD induction serum phosphorus plateaued at a concentration

around 20 mg/dl, thereby confirming the development of a stable hyperphosphatemia. At this time point, a decreased phosphate excretion was also observed in CKD rats. The phosphaturic hormone FGF23 was dramatically increased from week 4 of CKD onwards and peaked after 8 weeks of CKD to levels that were 500-fold higher as compared to control values.

Inherent to CKD, serum calcium concentrations of CKD rats were significantly lower as compared to control rats with normal renal function during the entire study period. The established hypocalcemia is consistent with the increased calcium loss via the urine in CKD rats from week 4 onwards, indicating the impaired capacity of the kidney to reabsorb calcium.

Hypocalcemia and hyperphosphatemia resulted in the establishment of secondary hyperparathyroidism as indicated by the dramatic 20-fold increase in serum PTH levels.

Vascular calcification

The total calcium content in the aorta was significantly increased from 4 weeks after CKD induction onwards in comparison with rats with normal renal function. However, after 8 weeks of renal failure calcium concentrations in the aorta and the carotid and femoral arteries were strongly increased, but did not further augment in the following weeks (Figure 1 panel A, B and C).

Determination of the percentage calcified tissue on von Kossa stained sections of the aorta showed that the calcified area increased after 8 weeks of CKD with significant differences from week 10 onwards (Figure 1 panel D). Figure 4 exhibit representative photos of aortic sections stained with von Kossa to visualize calcified areas in the vessel wall in control rats (4A) as well as CKD rats at week 8 (4D) and 12 (4G). No calcification is detected in aortas of control rats whereas circumferential, severe calcification is present in CKD rats after 8 and 12 weeks.

Calcification in the aorta was significantly correlated with serum creatinine ($r=0.61$, $p<0.001$), phosphate ($r=0.66$, $p<0.001$), PTH ($r=0.81$, $p<0.001$) and FGF23 ($r=0.72$, $p<0.001$).

Disturbances in bone turnover

Both static and dynamic bone parameters are presented in figures 2 and 3, respectively. In general, no differences in bone area, mineralized area and trabecular thickness were noted at the different time points, with exception of the CKD group that was sacrificed after 4 weeks of CKD, which showed significant lower values of the respective bone parameters as compared to control animals. The osteoid area rose with the duration of CKD with significant elevated values after 8 and 10 weeks; the osteoid width followed a similar pattern, however, significance was only reached after 12 weeks of CKD. Inherent to CKD, both the osteoclast and eroded perimeter were significantly increased from 10 weeks of CKD onwards in comparison with rats with normal kidney function. Finally, the osteoblast perimeter was also markedly expanded which is another hallmark of CKD-related hyperparathyroid bone disease.

Concerning the dynamic bone parameters, measurement of the tetracycline labels on unstained sections of the tibia revealed that in a number of the rats sacrificed after 10, 11 and 12 weeks of CKD, denoted in figure 3, dynamic bone parameters could no longer be measured, because of chaotic incorporation of tetracycline labels. Nevertheless, after 4 and 8 weeks on a 0.25% adenine/low vitamin K diet, all rats had a measurable, significantly increased bone formation rate and mineral apposition rate. CKD rats also exhibited an increasing trend in mineralization lag time, but no significant differences with control rats were found for this parameter.

Figure 4 shows Goldner stained tibial sections and unstained sections with tetracycline labels visualized by fluorescence microscopy of both control and CKD rats. Goldner stained sections of the tibia demonstrate increased osteoid, resorption lacunes and the presence of fibrosis in trabecular bone of CKD rats (4E and H), indicative for high bone turnover, as compared to control rats (4B). After 8 weeks of CKD two lines of tetracycline labels, incorporated into mineralizing bone at two time points before sacrifice, can be distinguished (4F), whereas after 12 weeks of CKD labels are chaotically incorporated and thus not measurable as a result of excessive bone turnover (4I).

Relationship between vascular calcification and bone metabolism

Spearman univariate analysis between the aortic calcium content and all bone parameters measured revealed that a significant correlation exists between aortic calcification on the one hand and osteoid area, osteoid perimeter, osteoid width, eroded perimeter, osteoblast and osteoclast perimeter, mineral apposition rate, bone formation rate and mineralization lag time on the other hand (Table 2). Multiple regression analysis showed that the eroded perimeter and the mineral apposition rate are significant predictors for the development of aortic calcification. 52% of the variation in the aortic calcium content can be explained by these two bone parameters (Table 2).

Aortic mRNA expression of proteins involved in cell senescence, the FGF23-klotho axis and osteogenesis

Induction of CKD in rats did not alter the mRNA expression of prelamin A and FACE1, two proteins involved in vascular smooth muscle cell senescence (figure 5). In addition, no changes in expression of FGF23, klotho, FGFR1 or FGFR3 were found between CKD and control animals (figure 5). Of particular interest, FGF18 expression was significantly lower after 11 weeks of CKD as compared to rats with normal renal function of similar age (Mann Witney U test, $p=0.01$). FGF18 expression also negatively correlated with serum creatinine levels at sacrifice (Spearman correlation, $r=-0.4$ $p<0.01$). Uremia also did not modulate the mRNA expression of sclerostin, the SOST gen product that inhibits the wnt signaling pathway, a regulatory pathway involved in osteoblast differentiation. Only FGF18 expression negatively correlated with the calcium content in the aorta (Spearman correlation, $r(s)= -0.3$ $p<0.03$).

Discussion

Patients with impaired renal function exhibit dysregulated biochemical parameters of the mineral metabolism such as abnormal calcium, phosphorus, PTH, vitamin D and FGF23 levels that give rise to renal osteodystrophy and extraosseous calcification particularly in the arteries. This clinical

syndrome associated with chronic renal impairment is called Chronic Kidney Disease-Mineral and Bone Disorder (CKD-MBD). A disturbed bone turnover, either low or high, and vascular calcification develop as a consequence of CKD but are also related to each other, known as the calcification paradox: disturbed physiological bone mineralization is associated with a higher risk of pathological calcification in the arterial wall (4). The relationship between bone mineralization and vessel calcification is also accentuated by the cell biological similarities in both processes (12). Hence, it is of the utmost importance to assess whether innovative therapies focusing on the direct interference with the formation of calcified nodules in the arteries, such as pyrophosphate, do not coincide with a negative impact on bone formation or mineralization.

Up to now, no valuable rodent model to study CKD-related bone pathology and vascular calcification concomitantly is available. ApoE KO mice with superimposed CKD are used for studies on vascular calcification and bone disease (13;14). However, this experimental model develops rather mild CKD and involves the development of atherosclerosis due to disturbances of the lipid metabolism, and in particular develops intimal calcifications in atherosclerotic plaques with limited medial calcifications. Some years ago, the group of Moe presented the heterozygous Cy/+ rat with polycystic kidney disease as a model of CKD-MBD in which 60% of the animals developed mild to severe aortic calcifications after 38 weeks and abnormal bone changes based on static bone measurements (15). The slow progression of CKD and therefore the late onset of the calcification in the arteries (between 34-38 weeks of age) as well as the limited reproducibility makes this rat model less suitable for being used in interventional studies. Alternatively, the 5/6th nephrectomy rat model, generally used to evaluate CKD-induced bone disease, only sporadically develops arterial calcification unless they are exposed to supra-physiological doses of vitamin D which in itself may also influence bone metabolism. The latter rat model displays a rather mild degree of renal impairment, yet, a relatively high mortality is noticed in this surgically induced CKD model. On the other hand, the conventional adenine-induced CKD rat model (0.75% adenine-low protein diet for 4 weeks) , routinely used to study CKD-induced vascular calcification, entails

the disadvantage of chaotic mineralization of the osteoid leading to immeasurable dynamic bone parameters such as bone formation rate and mineralization lag time. Dynamic bone parameters are indispensable to verify whether or not therapeutic agents affect physiologic bone parameters. Moreover with the conventional adenine rat model renal function partially restores after stop of adenine treatment which makes it difficult to differentiate between effects related to treatment versus those associated with amelioration of renal function.

Last year, Shobeiri et al. (16) presented a modified adenine-induced CKD rat model consisting of the incessant addition of a lower dietary 0.25% adenine content and the reduction of vitamin K content by about 25 times in order to induce CKD-related vascular calcification. They found a 100% incidence of abdominal calcification with increased pulse pressure and decreased diastolic pressure after 11 weeks of CKD, but bone status was not analyzed in this model. In the current study, a similar adenine enriched low vitamin K diet was used to study CKD-related vascular calcification and bone disease. A stable severe CKD was induced as indicated by the rise in serum creatinine levels to values plateauing at 5 mg/dl. Along with these changes indicative for serious renal dysfunction a stable hyperphoshatemia and hypocalcemia developed which is inherent to CKD and resulted in increased serum PTH concentrations. Serum FGF23 levels were dramatically increased prior to significant changes in serum phosphate levels which is also observed in CKD patients (17). The incessant administration of 0.25 % dietary adenine with low vitamin K led to a significant increased calcium content in the aorta and peripheral arteries. All CKD animals had higher arterial calcium concentrations as compared to rats with normal renal function although a relative variability in degree of calcification was notable. The mean calcium content in the aorta and carotid artery still increases beyond 8 weeks as does the Von Kossa positive area in the aorta, whereas the calcium content of the femoral artery slightly fluctuates after 8 weeks of CKD. Therefore, the current CKD model can be considered as a valuable rat model to study bone and vessels for up to 8 weeks, however might limit the applicability for longer term drug studies. At first sight it seems rather peculiar that vascular calcification in the CKD rat develops with

hypocalcemia, which occurs because of decreased intestinal calcium absorption due to lower $1,25(OH)_2$ vitamin D_3 production in damaged kidneys. Nevertheless, calcification of the vessels in the CKD animals is the result of the excessive phosphorus levels in the serum, which is generally accepted as a major driver of vascular calcification. Calcification in this CKD rat model is located in the medial layer. Local inflammation is believed not to play a major role in this type of calcification, in contrast to its proven role in atherosclerosis-related calcification, as no leucocyte infiltrates were found on OX-1 stained sections of calcified vessels of the conventional adenine-induced CKD model (unpublished results).CKD-related bone disease had also developed as reflected by the increased osteoblast and osteoclast perimeter along with a rise in an increased osteoid and eroded surface. Dynamic bone parameters, particularly bone formation rate and mineral apposition rate, show that bone disturbances arise early in this rat model, i.e. at 4 weeks of CRF. Continuous administration of an adenine low vitamin K diet for 10 weeks or more resulted in chaotic incorporation of the tetracycline labels in the bone whereby dynamic bone parameters cannot be calculated in a substantial fraction of the CKD rats. These findings indicate that feeding of rats with an adenine enriched low vitamin K diet for up to 8 weeks leads to a stable renal impairment and is a valuable experimental model to study CKD-related vascular calcification and bone pathology concomitantly in one and the same animal. As such, this rat model is the first to allow us to compare the effect of new treatment strategies on the onset and further progression of vascular calcification and to evaluate their (possibly detrimental) effect on bone mineralization and metabolism.

In order to investigate the relationship between disturbed bone metabolism and vascular calcification, multiple regression analysis was performed to test whether aortic calcification can be predicted by bone parameters. We found that the calcium content in the aorta can be predicted to a significant extent by the eroded perimeter and the mineral apposition rate, which is the rate by which osteoid is mineralized. Whilst an increased eroded perimeter points to an enhanced efflux of phosphorus and calcium out of the bone, thus resulting in increased amounts of both minerals in

circulation which in turn will induce conversion of vascular smooth muscle cells (18;19) towards bone-like cells and increase the deposition of hydroxyapatite crystals in the vessel wall, this may also lead to a more rapid mineral apposition in the bone. Further studies are needed to find out to which extent not yet defined factors promoting/inhibiting the mineralization processes in both bone and vessels may support these observations. Results of the present study again underscore the importance of the state of the bone in the manifestation of vascular calcification which is in accordance to previous studies dealing with the calcification paradox (20-22). It is important to keep in mind that both high and low bone turnover diseases are associated with vascular calcification. In the CKD model of this study only high bone turnover is represented which may be considered as a limitation of this study. In view of these results, it is of utmost importance to evaluate both bone metabolism and vascular complications when new treatments for either vascular calcification or disturbed bone metabolism are being studied.

This alternative CKD rat model was also used to investigate the aortic expression of proteins that play a role in cell senescence, the FGF23-klotho axis and the wnt signaling pathway which are all suggested to be involved in arterial calcification. A hallmark of vascular smooth muscle cell senescence consists of the downregulation of FACE1 and the rapid accumulation of prelamin A, which undergoes posttranslational modification and cleavage by the metalloprotease Zmpste24/FACE1 to become the mature nuclear intermediate filament lamin A (23). Liu et al (24) have demonstrated that prelamin A is highly deposited in calcified arteries of young children on dialysis and that prelamin A accelerates vascular smooth muscle cell calcification and osteogenic reprogramming of the cells. In our study, however, no altered expression of both senescence-associated genes was noted in CKD animals as compared to rats with normal renal function and no differential expression of FACE1 and prelamin A was seen between animals that were or were not calcified in the aorta. Apparently, CKD-induced vascular calcification in our rat model was not mediated or accelerated by cell senescence. Ragnauth et al (23) showed that oxidative stress induces cell senescence. As oxidative stress is related to inflammation and duration of dialysis treatment

(25), it is plausible that cell senescence is involved in arterial calcification once CKD patients undergo dialysis, which is known to induce an inflammatory state. In adenine-induced CKD rats neither systemic nor local inflammation in the arteries is present which might explain the lack of changes in mRNA expression of genes that contribute to cell senescence in calcified aortas of CKD animals. However, the role of cell senescence in vascular calcification needs to be further elucidated in patients across different CKD stages.

Sclerostin is produced by osteocytes and functions as an inhibitor of the wnt/β-catenin pathway which controls osteogenesis and the terminal differentiation of osteoblasts. Aside from its function in the bone, there is growing evidence that sclerostin might be involved in vascular calcification. Serum sclerostin is positively associated with the extent of aortic valve calcification and abdominal aortic calcification in CKD and hemodialysis patients (26;27) and postmenopausal women (28), respectively. However, with regard to local sclerostin expression in the arteries, little is known. Increased sclerostin expression was observed in calcified human aortic valves (29). Zhu et al. (30) also found increased protein expression of sclerostin in the calcified media of Enpp1 knockout mice aortic tissue. Nevertheless, in our study CKD induction in rats did not change aortic sclerostin mRNA expression and no different sclerostin expression was observed between calcified and non-calcified aortas. The role of sclerostin in vascular calcification, be it either protective or harmful, and in the interplay between the bone-vascular axis is far from being known and is still anticipating elucidation. Our study supports the fact that sclerostin produced by vascular cells does not play a major role in vessel calcification.

The FGF23/klotho axis is well known to regulate phosphate homeostasis. The phosphaturic hormone FGF23 interacts with FGF receptors in the kidney, most prominently FGFR1, and requires klotho as a co-receptor for receptor activation. Growing interest is nowadays poring on the role of the FGF23/klotho axis in the onset or progression of vascular calcification. In CKD, serum FGF23 levels excessively rise whereas renal and vascular klotho expression declines, which both appear to be associated with increased cardiovascular disease and calcification (31-33). With regard to

vascular expression of FGF23, klotho and FGFRs in both normal versus CKD conditions too little is known and inconsistency exists. In human coronary arteries, FGF23 was detected, particularly in calcium positive areas (34), however, Donate-Correa et al. did not observe mRNA FGF23 expression in aortic human specimens (35). In rodents, controversy on FGF23 expression in the vasculature also exists. Zhu et al. (36) found no FGF23 expression in aortas of wild-type mice, but deletion of Enpp1 in mice showed increased expression of this hormone in calcified aortas. On the other hand, LDLR knockout mice exhibit significant aortic FGF23 expression, but induction of CKD reduced it (32). In our study FGF23 mRNA expression was found in normal rats and did not change by induction of severe CKD. This large heterogeneity on data regarding arterial FGF23 expression calls for more extensive research in different diseases (such as CKD, vascular calcification, cardiovascular disease) as well as healthy conditions in various vessel types and species in order to assign a role for this hormone in the vasculature.

With regard to klotho expression, studies are unanimous in the presence of klotho mRNA and protein in human vessels (31;34;35). In CKD patients, klotho protein expression was markedly reduced which was associated with extensive medial calcification (31). Reduced klotho expression in aortas from LDLR knockout mice with induced CKD confirms that CKD leads to vascular klotho deficiency (32). However, despite a decreasing trend, adenine-induced severe CKD did not significantly alter aortic klotho mRNA expression in the current study, which supports data in another CKD rat model (37). The discrepancy in these results may be explained in part by the finding that inflammation is a major suppressor of klotho expression (31;38). CKD rat models do not exhibit inflammation, whereas LDLR knockout mice and end stage CKD patients are characterized by an inflammatory state that can affect tissue klotho expression. These recent data point towards a putative role of klotho in vascular calcification, especially in the context of dialysis where inflammation is present.

In our CKD rat model, abundant mRNA expression of FGFR1 and FGFR3 was found in the aorta, but CKD did not influence the mRNA levels and no association between calcification and

expression and FGFR mRNA was detected. This observation extends studies reporting the presence of both FGFRs in human vascular tissue (31;34;35). Decreased FGFR1 and FGFR3 have been reported in calcified aorta of Enpp1 knockout mice (36) and CKD patients (31).

FGF18 also acts via FGFR2 and FGFR3 to regulate chondro- and osteogenesis in the bone. Since FGF18 is also expressed in human cardiovascular tissue (39) and osteochondrogenesis is a well described phenomenon contributing to vascular calcification, we analyzed its expression in the aorta. We found significantly lower FGF18 expression in CKD rats as compared to controls and a negative correlation between FGF18 mRNA expression and aortic calcium content. As FGF18 is reported to be a direct target of the canonical wnt/β-catenin signaling (40), the reduced aortic FGF18 expression in CKD rats is in agreement with previous findings in our lab which demonstrated a reduced expression pattern of the wnt/β-catenin signaling in calcified aorta of a similar CKD rat model (9) and with increased circulating sclerostin levels in patients with vascular calcification (26;27). To the best of our knowledge, this study is the first one to report an (negative) association between aortic FGF18 expression and aortic calcium content. Further in vitro research is required to figure out whether FGF18 is important in the process of vascular calcification and whether it might play a role in CKD-related bone disease.

In general, this presented rat model with stable CKD develops moderate vascular calcification and quantifiable bone pathology, meaning that both static and dynamic bone parameters can be measured which is indispensible for complete interpretation of bone metabolism and was an important shortcoming of previous CKD rat models used to study vascular and bone disease, and thus lends itself to study these two main complications concomitantly in one and the same animal. In the future, this CKD model will be valuable to study the effect of innovative therapies for treatment of vascular calcification on both the vasculature and bone metabolism and to further explore the mechanisms underlying the calcification paradox.

Acknowledgments

Ellen Neven and Anja Verhulst are postdoctoral fellows of the Fund for Scientific Research–Flanders (FWO). We especially thank Hilde Geryl, Ludwig Lamberts, Rita Marynissen and Simonne Dauwe for their excellent technical assistance and Dirk De Weerdt for his help with the graphics. Authors' roles: EN, RBD, GD, GJB, AV and PCD contributed to conception and study design, data acquisition and interpretation. ME has significantly contributed to statistical analysis and interpretation of the results. EN has written the manuscript. AV, GB and PCD have revised and approved the final version of the manuscript. EN and PCD take responsibility for the integrity of the data analysis.

References

(1) Sigrist MK, Taal MW, Bungay P, McIntyre CW. Progressive vascular calcification over 2 years is associated with arterial stiffening and increased mortality in patients with stages 4 and 5 chronic kidney disease. Clin J Am Soc Nephrol 2007;2(6):1241-8.

(2) Kalantar-Zadeh K, Shah A, Duong U, Hechter RC, Dukkipati R, Kovesdy CP. Kidney bone disease and mortality in CKD: revisiting the role of vitamin D, calcimimetics, alkaline phosphatase, and minerals. Kidney Int Suppl 2010;(117):S10-S21.

(3) London GM, Guerin AP, Marchais SJ, Metivier F, Pannier B, Adda H. Arterial media calcification in end-stage renal disease: impact on all-cause and cardiovascular mortality. Nephrol Dial Transplant 2003;18(9):1731-40.

(4) Persy V, D'Haese P. Vascular calcification and bone disease: the calcification paradox. Trends Mol Med 2009;15(9):405-16.

(5) Towler DA. Arteriosclerosis, Bone Biology, and Calciotropic Hormone Signaling: Learning the ABCs of Disease in the Bone-Vascular Axis. J Am Soc Nephrol 2015;26(2):243-5.

(6) Neven E, Dams G, Postnov A et al. Adequate phosphate binding with lanthanum carbonate attenuates arterial calcification in chronic renal failure rats. Nephrol Dial Transplant 2009; 24:1790-9.

(7) De Schutter TM, Behets GJ, Geryl H et al. Effect of a magnesium-based phosphate binder on medial calcification in a rat model of uremia. Kidney Int 2013;83(6):1109-17.

(8) Block GA, Spiegel DM, Ehrlich J et al. Effects of sevelamer and calcium on coronary artery calcification in patients new to hemodialysis. Kidney Int 2005;68(4):1815-24.

(9) Neven E, Persy V, Dauwe S, De Schutter T, De Broe ME, D'Haese PC. Chondrocyte Rather Than Osteoblast Conversion of Vascular Cells Underlies Medial Calcification in Uremic Rats. Arterioscler Thromb Vasc Biol 2010; 30:1741-50.

(10) Price PA, Roublick AM, Williamson MK. Artery calcification in uremic rats is increased by a low protein diet and prevented by treatment with ibandronate. Kidney Int 2006;70(9):1577-83.

(11) Dempster DW, Compston JE, Drezner MK et al. Standardized nomenclature, symbols, and units for bone histomorphometry: a 2012 update of the report of the ASBMR Histomorphometry Nomenclature Committee. J Bone Miner Res 2013;28(1):2-17.

(12) Neven E, De Schutter TM, De Broe ME, D'Haese PC. Cell biological and physicochemical aspects of arterial calcification. Kidney Int 2011; 79:1166-77.

(13) Massy ZA, Ivanovski O, Nguyen-Khoa T et al. Uremia accelerates both atherosclerosis and arterial calcification in apolipoprotein E knockout mice. J Am Soc Nephrol 2005;16(1):109-16.

(14) Nikolov IG, Joki N, Nguyen-Khoa T et al. Chronic kidney disease bone and mineral disorder (CKD-MBD) in apolipoprotein E-deficient mice with chronic renal failure. Bone 2010;47(1):156-63.

(15) Moe SM, Chen NX, Seifert MF et al. A rat model of chronic kidney disease-mineral bone disorder. Kidney Int 2009;75(2):176-84.

(16) Shobeiri N, Pang J, Adams MA, Holden RM. Cardiovascular disease in an adenine-induced model of chronic kidney disease: the temporal link between vascular calcification and haemodynamic consequences. J Hypertens 2013;31(1):160-8.

(17) Isakova T, Wahl P, Vargas GS et al. Fibroblast growth factor 23 is elevated before parathyroid hormone and phosphate in chronic kidney disease. Kidney Int 2011;79(12):1370-8.

(18) Giachelli CM. Vascular calcification: in vitro evidence for the role of inorganic phosphate. J Am Soc Nephrol 2003;14(9 Suppl 4):S300-S304.

(19) Yang H, Curinga G, Giachelli CM. Elevated extracellular calcium levels induce smooth muscle cell matrix mineralization in vitro. Kidney Int 2004;66(6):2293-9.

(20) De Schutter TM, Neven E, Persy VP et al. Vascular calcification is associated with cortical bone loss in chronic renal failure rats with and without ovariectomy: the calcification paradox. Am J Nephrol 2011;34(4):356-66.

(21) Kiel DP, Kauppila LI, Cupples LA, Hannan MT, O'Donnell CJ, Wilson PW. Bone loss and the progression of abdominal aortic calcification over a 25 year period: the Framingham Heart Study. Calcif Tissue Int 2001;68(5):271-6.

(22) Naves M, Rodriguez-Garcia M, Diaz-Lopez JB, Gomez-Alonso C, Cannata-Andia JB. Progression of vascular calcifications is associated with greater bone loss and increased bone fractures. Osteoporos Int 2008; 19:1161-6.

(23) Ragnauth CD, Warren DT, Liu Y et al. Prelamin A acts to accelerate smooth muscle cell senescence and is a novel biomarker of human vascular aging. Circulation 2010;121(20):2200-10.

(24) Liu Y, Drozdov I, Shroff R, Beltran LE, Shanahan CM. Prelamin A accelerates vascular calcification via activation of the DNA damage response and senescence-associated secretory phenotype in vascular smooth muscle cells. Circ Res 2013;112(10):e99-109.

(25) Nguyen-Khoa T, Massy ZA, De Bandt JP et al. Oxidative stress and haemodialysis: role of inflammation and duration of dialysis treatment. Nephrol Dial Transplant 2001;16(2):335-40.

(26) Brandenburg VM, Kramann R, Koos R et al. Relationship between sclerostin and cardiovascular calcification in hemodialysis patients: a cross-sectional study. BMC Nephrol 2013; 14:219. doi: 10.1186/1471-2369-14-219.:219-14.

(27) Claes KJ, Viaene L, Heye S, Meijers B, D'Haese P, Evenepoel P. Sclerostin: Another vascular calcification inhibitor? J Clin Endocrinol Metab 2013;98(8):3221-8.

(28) Hampson G, Edwards S, Conroy S, Blake GM, Fogelman I, Frost ML. The relationship between inhibitors of the Wnt signalling pathway (Dickkopf-1(DKK1) and sclerostin), bone mineral density, vascular calcification and arterial stiffness in post-menopausal women. Bone 2013;56(1):42-7.

(29) Koos R, Brandenburg V, Mahnken AH et al. Sclerostin as a potential novel biomarker for aortic valve calcification: an in-vivo and ex-vivo study. J Heart Valve Dis 2013;22(3):317-25.

(30) Zhu D, Mackenzie NC, Millan JL, Farquharson C, Macrae VE. The appearance and modulation of osteocyte marker expression during calcification of vascular smooth muscle cells. PLoS One 2011;6(5):e19595.

(31) Lim K, Lu TS, Molostvov G et al. Vascular Klotho deficiency potentiates the development of human artery calcification and mediates resistance to fibroblast growth factor 23. Circulation 2012 ;125(18):2243-55.

(32) Fang Y, Ginsberg C, Sugatani T, Monier-Faugere MC, Malluche H, Hruska KA. Early chronic kidney disease-mineral bone disorder stimulates vascular calcification. Kidney Int 2014;85(1):142-50.

(33) Jimbo R, Shimosawa T. Cardiovascular Risk Factors and Chronic Kidney Disease-FGF23: A Key Molecule in the Cardiovascular Disease. Int J Hypertens 2014; 381082.

(34) van Venrooij NA, Pereira RC, Tintut Y et al. FGF23 protein expression in coronary arteries is associated with impaired kidney function. Nephrol Dial Transplant 2014;29(8):1525-32.

(35) Donate-Correa J, Mora-Fernandez C, Martinez-Sanz R et al. Expression of FGF23/KLOTHO system in human vascular tissue. Int J Cardiol 2013;165(1):179-83.

(36) Zhu D, Mackenzie NC, Millan JL, Farquharson C, Macrae VE. A protective role for FGF-23 in local defence against disrupted arterial wall integrity? Mol Cell Endocrinol 2013;372(1-2):1-11.

(37) Jimbo R, Kawakami-Mori F, Mu S et al. Fibroblast growth factor 23 accelerates phosphate-induced vascular calcification in the absence of Klotho deficiency. Kidney Int 2014;85(5):1103-11.

(38) Moreno JA, Izquierdo MC, Sanchez-Nino MD et al. The inflammatory cytokines TWEAK and TNFalpha reduce renal klotho expression through NFkappaB. J Am Soc Nephrol 2011;22(7):1315-25.

(39) Antoine M, Wirz W, Tag CG et al. Fibroblast growth factor 16 and 18 are expressed in human cardiovascular tissues and induce on endothelial cells migration but not proliferation. Biochem Biophys Res Commun 2006 ;346(1):224-33.

(40) Reinhold MI, Naski MC. Direct interactions of Runx2 and canonical Wnt signaling induce FGF18. J Biol Chem 2007;282(6):3653-63.

Figure legends

Figure 1: Calcium content of the (A) aorta, (B) femoral artery, (C) carotid artery and (D) % calcified aortic area of rats with normal renal function (CTR) or with chronic kidney disease (CKD). Black dots with a white stripe represent rats that died before the planned sacrifice. w: week. *p < 0.05 versus CTR.

Figure 2: Static bone parameters in rats with normal renal function (CTR) or with chronic kidney disease (CKD): (A) bone area, (B) mineralized area, (C) osteoid area, (D) osteoid width (E) trabecular thickness, (F) eroded perimeter, (G) osteoblast perimeter and (H) osteoclast perimeter. w: week. *p < 0.05 versus CTR.

Figure 3: Dynamic bone parameters in rats with normal renal function (CTR) or with chronic kidney disease (CKD): (A) bone formation rate, (B) mineral apposition rate and (C) mineralization lag time. w: week. *p < 0.05 versus CTR. In part of the CKD animals sacrificed at week 10, 11 and 12 (displayed as percentage) dynamic bone parameters were not measurable because of the excessive high bone turnover and thus no value could be assigned to those animals.

Figure 4: Von Kossa stained sections of the aorta (A-D-G), Goldner stained sections of the tibia (B-E-H) and tetracycline labels of the bone (C-F-I) in rats with normal renal function (CTR) or with chronic kidney disease (CKD) at week 8 and 12.

Figure 5: mRNA expression profiles of genes involved in cell senescence, the FGF23-klotho axis and osteogenesis in the abdominal aorta of rats with normal renal function (CTR) versus those with chronic kidney disease (CKD) at different time points. * p< 0.05 versus CTR.

Table 1: Serum and urinary parameters of renal function and mineral metabolism in control rats with normal renal function (CTR) and chronic kidney disease (CKD). *p < 0.05 versus CTR, same time point; °p < 0.05 versus week 0, same study group; †p<0.05 versus CTR week 11.

			week 0	week 2	week 4	week 6	week 8	week 10	week 11
serum	creatinine	CTR	0.58 ± 0.05	0.65 ± 0.05	0.78 ± 0.07	0.79 ± 0.06	0.82 ± 0.08	0.66 ± 0.03	0.75 ± 0.06
	(mg/dl)	CKD	0.61 ± 0.07	1.05 ± 0.13*°	2.02 ± 0.49*°	5.14 ± 1.05*°	5.15 ± 1.10*°	5.23 ± 1.17*°	4.94 ± 0.80*°
	phosphorus	CTR	7.6 ± 1.1	8.2 ± 1.5	7.2 ± 1.0	5.5 ± 2.1	7.9 ± 1.5	6.5 ± 0.9	6.6 ± 1.6
	(mg/dl)	CKD	8.2 ± 1.3	8.2 ± 1.3	9.9 ± 4.4	18.7 ± 3.1*°	18.8 ± 2.8*°	19.7 ± 2.7*°	18.8 ± 3.9*°
	calcium	CTR	15.1 ± 0.7	13.7 ± 0.5	11.9 ± 0.6	11.1 ± 0.3	11.8 ± 0.6	10.3 ± 0.3	9.8 ± 0.9
	(mg/dl)	CKD	14.5 ± 0.8	13.0 ± 0.5*°	11.1 ± 1.2°	9.7 ± 1.2*°	7.6 ± 0.8*°	6.4 ± 0.7*°	6.8 ± 1.0*°
	PTH	CTR							1111 ± 425
	(pg/ml)	CKD			3691 ± 2218		15589 ± 5441†	23418 ± 3518†	21185 ± 4404†
	FGF-23	CTR							0.66 ± 0.11
	(ng/ml)	CKD			46.7 ± 111.3†		306.9 ± 303.3†	146.7 ± 349.2†	52.9 ± 89.9†
Urinary	phosphate	CTR	62 ± 14	181 ± 66	139 ± 55	153 ± 49	205 ± 91	92 ± 16	115 ± 119
	(mg/24hr)	CKD	79 ± 20	104 ± 60*	176 ± 87	107 ± 68	71 ± 63*	60 ± 30*	65 ± 19
	calcium	CTR	2.54 ± 1.44	1.04 ± 0.34	0.89 ± 0.37	1.28 ± 0.31	1.45 ± 0.89	1.17 ± 0.36	1.08 ± 0.80
	(mg/24hr)	CKD	2.09 ± 1.02	0.82 ± 0.28°	1.64 ± 1.31	2.26 ± 0.57*	1.92 ± 0.64	1.67 ± 1.00	1.80 ± 0.64*

Table 2: Univariate and multivariate analysis for aortic calcium content as dependent variable and bone parameters as independent variables.

Independent variable	Univariate analysis Dependent variable: calcium content aorta		Independent variable	Multivariate analysis* Dependent variable: calcium content aorta		
	r(s)	p-value		B	beta	p-value
Bone area	0.079	0.589				
Osteoid area	0.404	0.004				
Osteoid perimeter	0.394	0.005				
Eroded perimeter	0.603	0.000	Eroded perimeter	0.329	0.310	0.023
Mineral apposition rate	0.642	0.000	Mineral apposition rate	0.369	0.360	0.009
Bone formation rate	0.566	0.000				
Mineralization lag time	0.566	0.000				
Osteoid Width	0.306	0.032				
Osteoblast perimeter (relative to total perimeter)	0.486	0.000				
Osteoclast perimeter (relative to total perimeter)	0.572	0.000				
Trabecular thickness	0.174	0.233				
Mineralized area	0.066	0.653				

Multiple regression analysis was corrected for serum creatinine. * R square is 0.52.

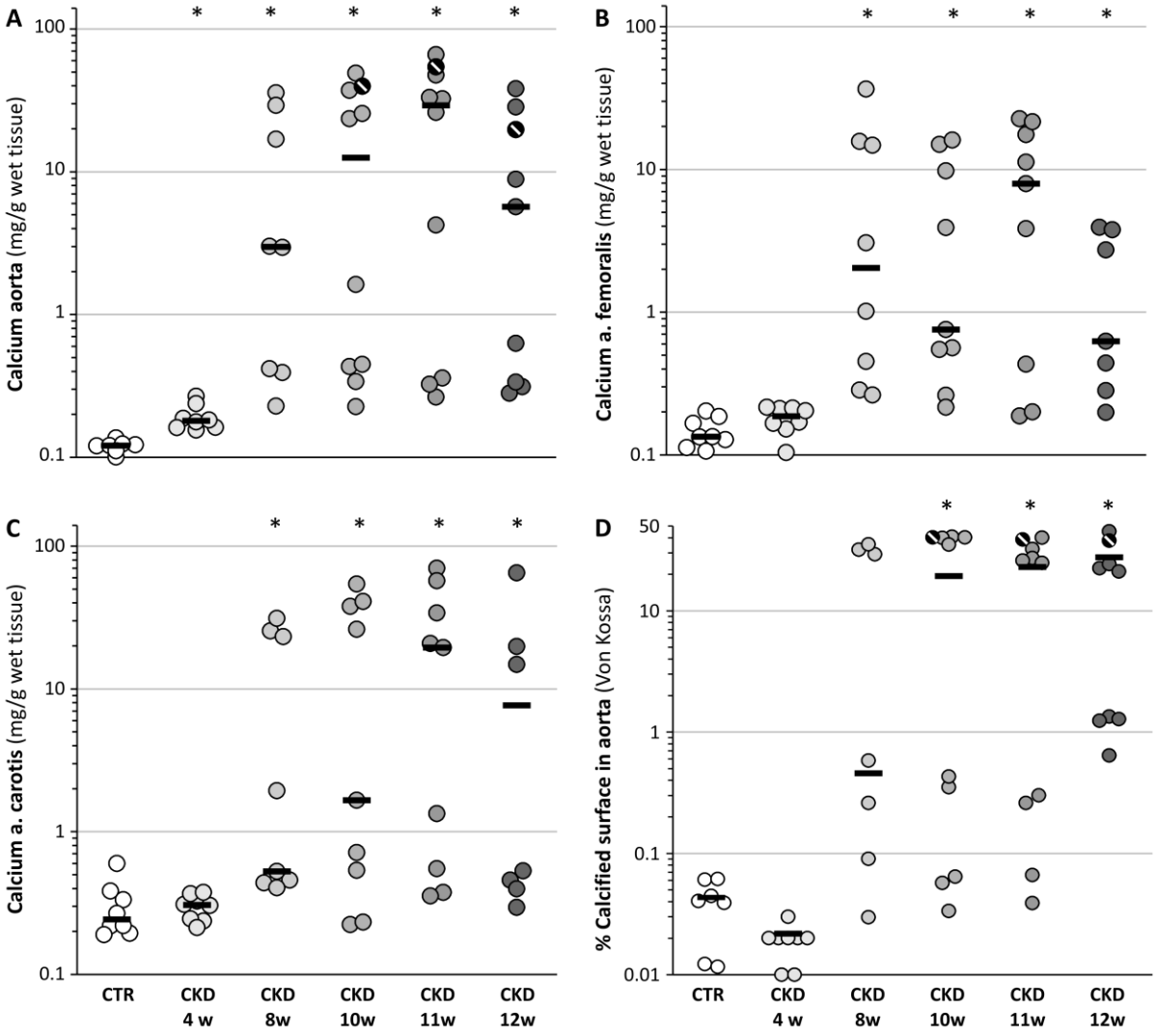

Figure 1

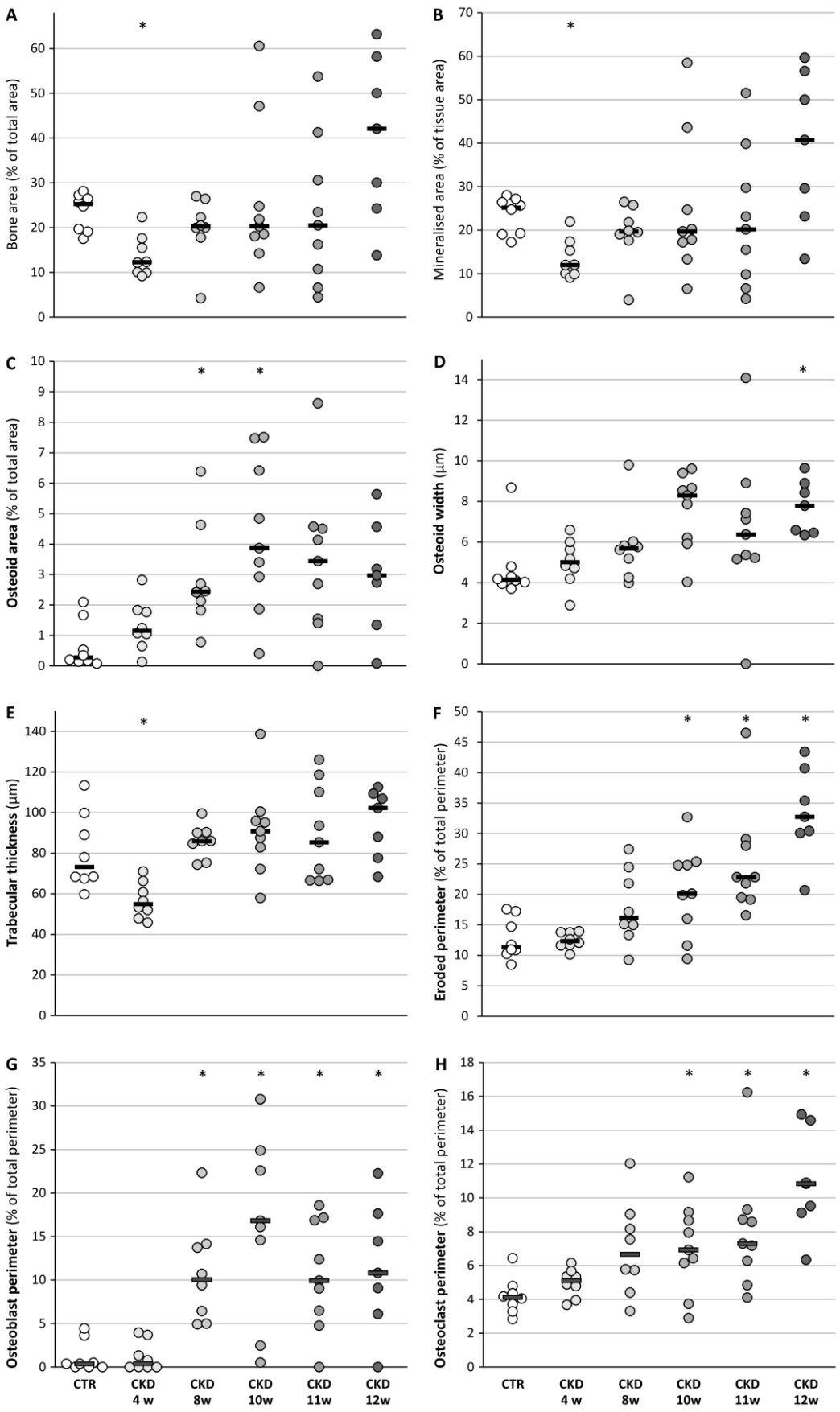

Figure 2

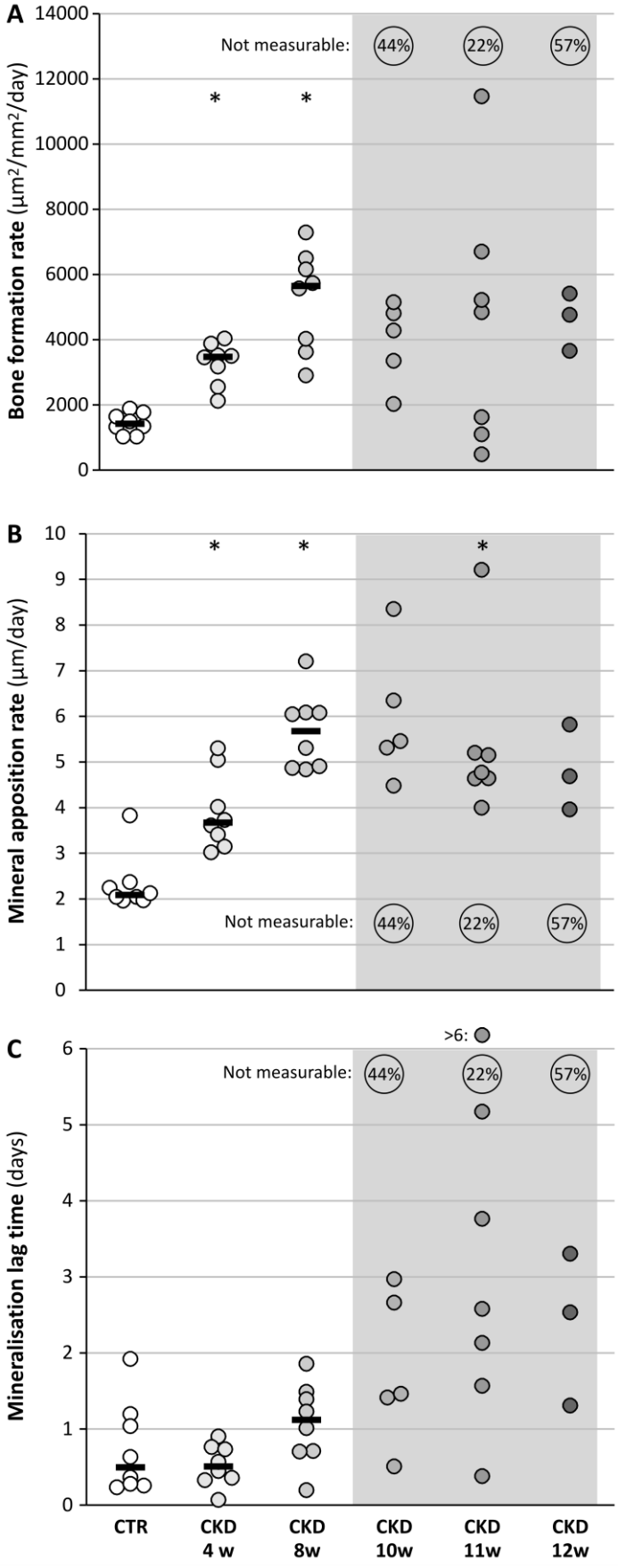

Figure 3

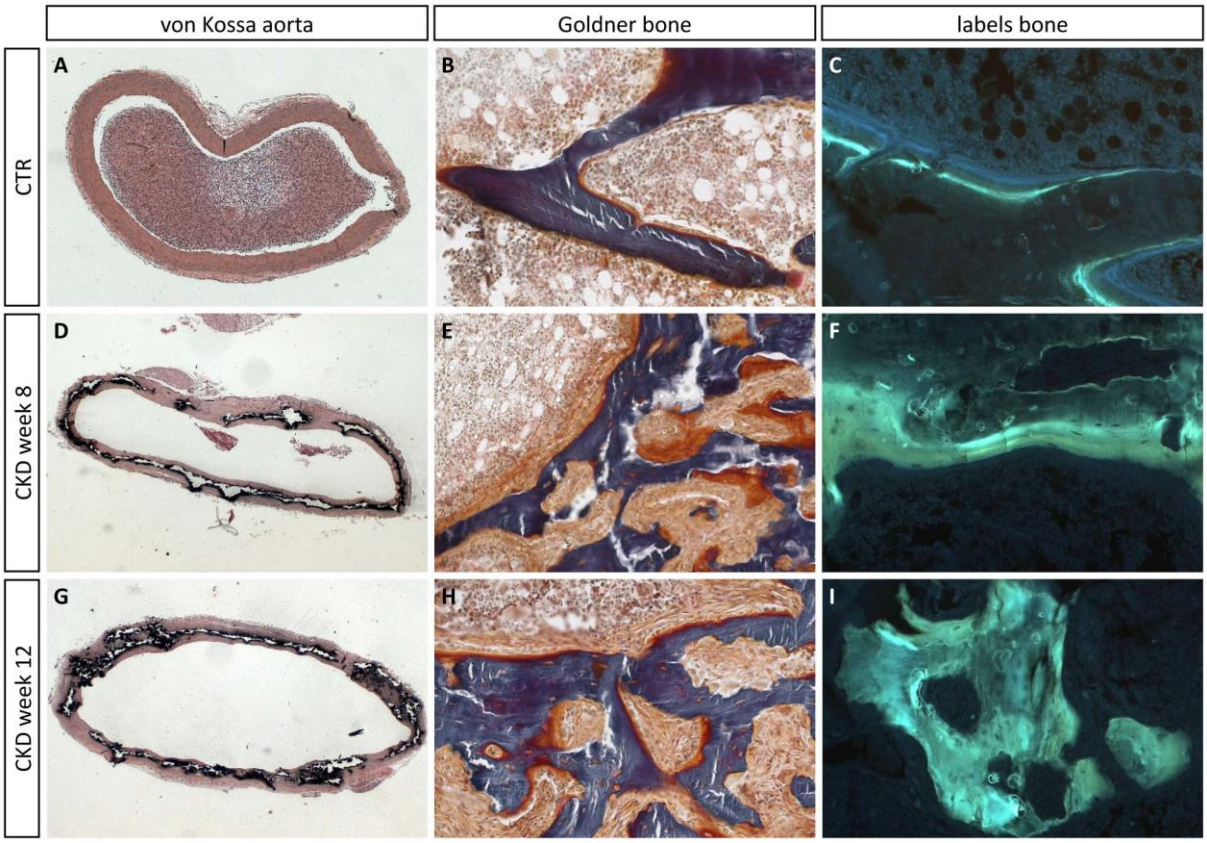

Figure 4

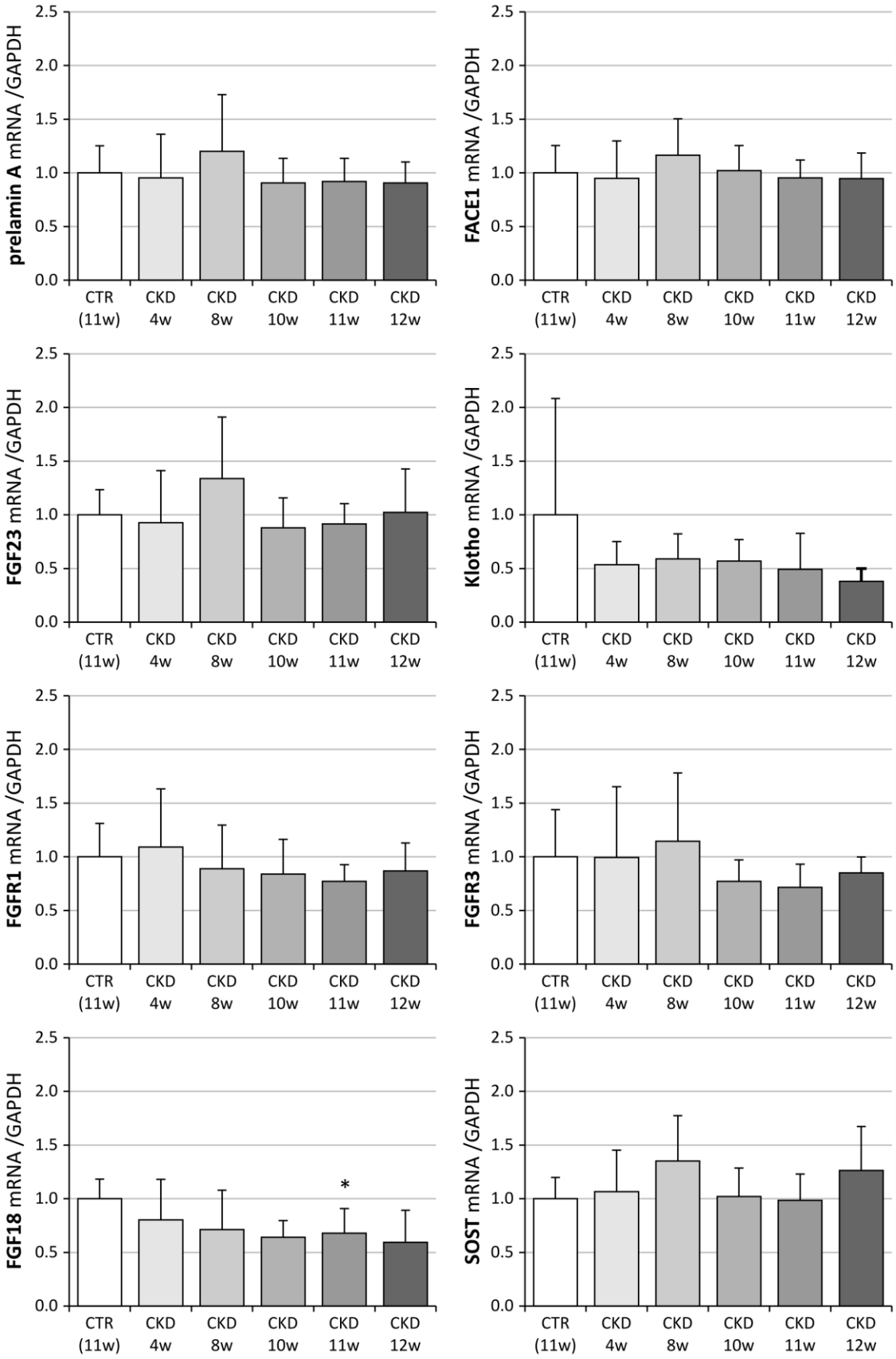

Figure 5